Density and production of NH and NH2 in an Ar-NH3 expanding plasma jet

Density and production of NH and NH_2 in an Ar–NH_3 expanding plasma jet

P. J. van den Oever,[a] J. H. van Helden, C. C. H. Lamers, R. Engeln, D. C. Schram, M. C. M. van de Sanden, and W. M. M. Kessels[b]
Department of Applied Physics, Eindhoven University of Technology, P.O. Box 513, 5600 MB Eindhoven, The Netherlands

(Received 2 February 2005; accepted 21 September 2005; published online 1 November 2005)

The densities of NH and NH_2 radicals in an Ar–NH_3 plasma jet created by the expanding thermal plasma source were investigated for various source-operating conditions such as plasma current and NH_3 flow. The radicals were measured by cavity ringdown absorption spectroscopy using the (0,0) band of the $A\,^3\Pi \leftarrow X\,^3\Sigma^-$ transition for NH and the (0,9,0)-(0,0,0) band of the $\tilde{A}\,^2A_1 \leftarrow \tilde{X}\,^2B_1$ transition for NH_2. For NH, a kinetic gas temperature and rotational temperature of 1750 ± 100 and 1920 ± 100 K were found, respectively. The measurements revealed typical densities of 2.5×10^{12} cm^{-3} for the NH radical and 3.5×10^{12} cm^{-3} for the NH_2 radical. From the combination of the data with ion density and NH_3 consumption measurements in the plasma as well as from a simple one-dimensional plug down model, the key production reactions for NH and NH_2 are discussed. © *2005 American Institute of Physics*. [DOI: 10.1063/1.2123371]

I. INTRODUCTION

Ammonia (NH_3) plasmas have widespread applications in research and industry for the (surface) treatment of materials. NH_3 plasmas are, for example, used for modifying the wettability and biocompatibility of polymers,[1–3] for improving the gas permeability of membranes,[4] for inducing surface passivation of electronic devices,[5,6] and for nitridation of dielectric and metallic materials.[7,8] Ammonia is also admixed in plasmas used for the synthesis of carbon nanotubes[9,10] and for ligand abstraction and nitridation during atomic layer deposition of metal nitrides.[11–13] One of the most important applications of NH_3-based plasmas in industry to date is, however, the deposition of silicon nitride films. These films—generally deposited from ammonia-silane plasmas—have numerous applications, ranging from dielectric materials in the microelectronics industry to antireflection coatings for crystalline silicon-based photovoltaics[14,15] and encapsulation films for organic light-emitting diodes.[16]

Despite their widespread application, only few experimental studies on the plasma chemistry in NH_3-based plasmas have been reported. Miller and Baird have addressed the plasma decomposition of NH_3 in radio-frequency plasmas,[17] while Pringle *et al.* have addressed the ion chemistry in a helical resonator.[18] These studies have not addressed the chemistry involved in ammonia radical production in detail. These radical species, however, are very likely most important during surface treatment. The interaction of NH and NH_2 plasma radicals with the surface of different materials has been addressed by Fisher and co-workers, using a molecular plasma beam in combination with laser-induced fluorescence for radical imaging.[19–21] Laser-induced fluorescence has also been used for determining the density of NH and NH_2 produced by NH_3 decomposition on a heated tungsten filament.[22] For depositing systems, few studies of the NH_3 plasma chemistry using mass spectrometry have been reported, for example, for the ammonia-silane chemistry[23,24] and recently also for the ammonia-acetylene chemistry.[25] In both pure NH_3 plasmas and depositing plasmas, the chemistry is very complex and much remains unknown about the NH_3 dissociation and its products.

To obtain more insight into the chemical reactions involved in the dissociation of NH_3 in plasmas, we have investigated the NH_3 dissociation process with respect to NH and NH_2 radical production. These studies were carried out using the expanding thermal plasma (ETP) technique, whose remote operation leads to a relatively simple chemistry, which facilitates plasma chemical investigations. Besides the technological relevance for NH_3 plasma surface treatment, the investigations can also be of astrophysical relevance.[26,27] Our particular interest lies, however, primarily in gaining a better understanding of the ultrahigh-rate deposition process of silicon nitride films by the expanding thermal plasma,[15,28] in which silane is cracked by reactive ion and radical species (such as NH and NH_2) in the Ar–NH_3 plasma jet.

After presenting the basics of the ETP technique in Sec. II, we present the experimental details of the cavity ringdown measurements carried out to determine the NH and NH_2 radical densities (Sec. III). In Sec. IV, we present the measured NH and NH_2 radical densities as a function of NH_3 flow and current in the plasma source. Supported by data on the ion density and NH_3 consumption, we argue that NH_3 dissociation in the ETP technique is governed by Ar^+ ions emanating from the plasma source. For NH, the key chemical reactions are charge transfer of NH_3 with Ar^+ and dissociative recombination with electrons, while the NH_2 production appears to involve more reactions such as ion-molecule and H-abstraction reactions. This basic reaction mechanism is supported by a one-dimensional plug down model. The conclusions are presented in Sec. V.

[a]Electronic mail: p.j.v.d.oever@tue.nl
[b]Author to whom correspondence should be addressed; electronic mail: w.m.m.kessels@tue.nl

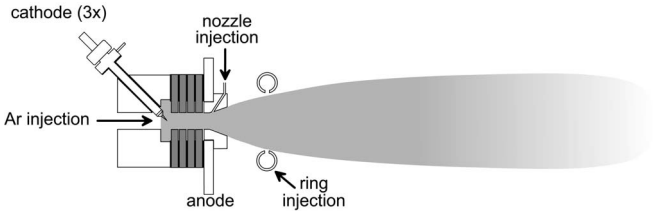

FIG. 1. Schematic representation of the expanding $Ar-NH_3$ plasma jet.

II. EXPANDING THERMAL PLASMA SETUP

The $Ar-NH_3$ plasma jet is produced using the ETP technique described extensively in the literature (see, e.g., Refs. 29 and 30). As shown in Fig. 1, this technique uses a cascaded arc plasma source to produce an Ar plasma at subatmospheric pressure (typically 400 kPa). In the cascaded arc, a dc current is drawn between three cathodes and one common grounded anode through a narrow (4 mm diameter) channel filled with argon gas. The cathode region and anode are separated by several " cascaded" plates, which are at floating potential. The plasma expands supersonically through a conically shaped nozzle into a low-pressure reactor (typical pressure is 20 Pa), and after a stationary shock at approximately 5 cm from the nozzle, the expansion continues subsonically. When going from supersonic to subsonic expansion, the directed velocity of the plasma changes from $\sim$1800 to $\sim$600 m/s. In the downstream region the electron temperature ($\sim$0.3 eV) is low, which can be attributed to the expansion and to the fact that no electrical power is coupled into the plasma in that region. Precursor gases can be injected into the Ar plasma jet, either through a slit in the nozzle or through an injection ring situated downstream in the jet.

In the present experiment, the plasma source is operated on pure Ar with a flow of 55 standard $cm^3\ s^{-1}$ (sccs), and the current through the arc channel is controlled between 30 and 70 A with a typical voltage of 40 V. The expanding Ar plasma was characterized in detail in our previous work and a brief description of some of the key findings is given here. In the downstream region, the Ar^+ ion and electron density are in the order of $10^{13}\ cm^{-3}$. The metastable argon density Ar^m is directly linked to the ion density but is typically lower by a factor of 10.[31] From the combination of radial ion density measurements and the forward velocity in the expansion, the equivalent flow of Ar^+ ions emanating from the source is estimated. For a current of 45 A, we found an "Ar^+ ion flow" of 2–3 sccs, corresponding to an average Ar ionization degree of $\sim$5% in the plasma source. Furthermore, the Ar^+ ion flow is found to increase linearly with the plasma current for a constant Ar flow through the source.[29,30]

Two injection locations of NH_3 molecules are used: NH_3 is either injected in the nozzle before the expansion or $\sim$7.5 cm downstream the expansion via a stainless-steel injection ring. The NH_3 flow range used is 0.5–17 sccs, and the downstream pressure is kept constant at 20 Pa by adjusting the gate valve to the pump. A substrate holder is positioned downstream at $\sim$39 cm from the source. Furthermore, besides the cavity ringdown system that will be discussed in detail in the next section, the setup is also equipped with a Langmuir probe,[29] that can measure ion and electron densities at $\sim$36 cm downstream from the source, and a residual gas analyzer for basic mass spectrometry measurements, which is situated at $\sim$56 cm from the source in the plasma beam.

III. CAVITY RINGDOWN SPECTROSCOPY ON NH AND NH_2

Cavity ringdown spectroscopy[32] (CRDS) was used to measure the density of the NH and NH_2 radicals in the downstream plasma at a position of 36 cm from the source. Briefly, CRDS is based on the injection of a laser pulse in a stable optical resonator (cavity) that consists of two high reflectivity mirrors. The decay rate of the light inside the resonator is detected through one of the mirrors. Cavity ringdown prevents the most common limitation of absorption measurements as the decay rate is independent of the intensity of the light pulse and is therefore not affected by pulse-to-pulse energy fluctuations of the laser system. For an "empty" cavity, this decay rate is simply determined by the reflectivity of the mirrors and the cavity length, but the decay rate becomes faster when absorbing (or scattering) species are present in the cavity. From the difference in decay rate between these two conditions, the absorption due to the species can be determined. Consequently, the number density of the species can be calculated when information on the cross section and absorption path length is available.

The cavity used in the present work consisted of plano-concave mirrors with a 100 cm radius of curvature and 2.5 cm diameter, placed 112 cm apart on flexible bellows. In front of the mirrors an Ar flow was injected to protect the mirrors from reactive plasma species. The NH radical was detected using high-reflectivity mirrors with a center-optimum reflectivity at 340 nm (Laser-Optik, $R=\sim0.998$), while for the NH_2 radical detection the center-optimum reflectivity was at 560 nm (Laser-Optik, $R=\sim0.999$). Laser light pulses were generated by a Sirah PrecisionScan-D dye laser pumped by the second harmonic of a Spectra-Physics GCR-4 Nd:yttrium aluminum garnet (YAG) laser working at a repetition rate of 10 Hz. For NH detection, Pyridine 1 laser dye was used to create $\sim$680 nm light, which was subsequently doubled to $\sim$340 nm by a potassium dihydrogen phosphate (KDP) crystal. For NH_2 detection, the $\sim$600 nm output of the dye laser operated on Rhodamine B laser dye was directly used. To avoid saturation of the transition of interest the amplifier stage of the dye laser was not used in the latter case. The laser intensity was further reduced by a set of filters while a UV attenuator was used for the 340 nm laser light. The typical pulse energy in front of the cavity was 100 μJ/pulse. Detection took place by means of a photomultiplier tube (Hamamatsu R928) at the other cavity mirror through a narrow bandpass filter, which blocked the plasma light. For every laser shot the photomultiplier signal was processed separately by a 100 MHz, 12 bits data-acquisition system [TU/eDACS (Ref. 33)]. All decay rates were single exponential and were analyzed by a weighted least-squares fit of the logarithmic of the transient data. To improve the signal-to-noise ratio an average of 20 ringdown times was

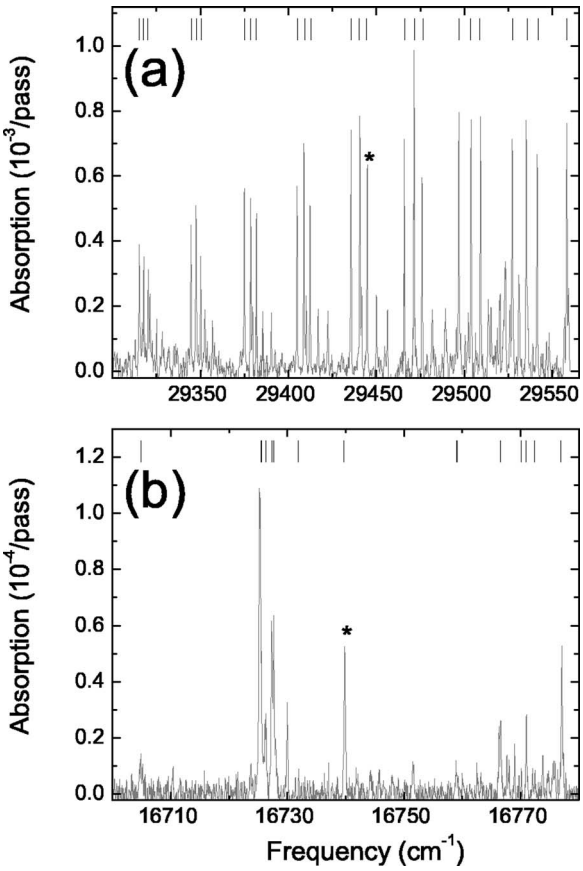

FIG. 2. Spectra of (a) NH and (b) NH_2 as measured with cavity ringdown spectroscopy. A plasma source current of 45 A and an NH_3 flow of 5 sccs are used for the measurements of the spectra. The absorption line positions reported in the literature are indicated in the upper part of the graphs, as are the absorption lines used for the density measurements (marked by an asterisk).

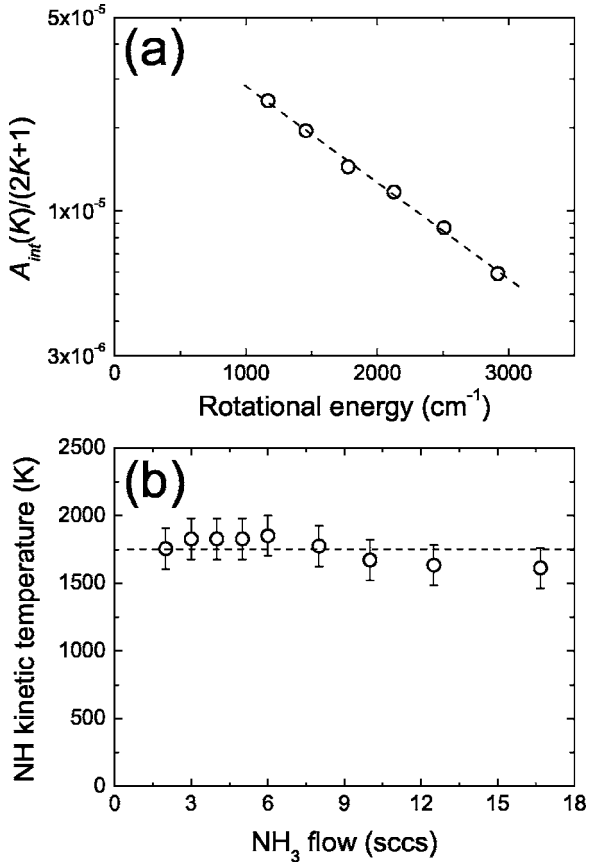

FIG. 3. (a) The statistically weighted integrated absorptions $A_{\mathrm{int}}(K)/(2K+1)$ for several rotational lines (P_{33} branch) of the (0,0) band of the $A\,^3\Pi \leftarrow X\,^3\Sigma^-$ transition of NH as a function of the rotational energy. The rotational temperature was determined from the slope of the linear fit (dashed line). (b) The kinetic temperature of the NH radical determined from the Doppler broadening of the $P_{33}(9)$ absorption line on the (0,0) band of the $A\,^3\Pi \leftarrow X\,^3\Sigma^-$ transition as a function of the injected NH_3 flow. The dashed line represents the average value.

taken for all measurements. The absorption loss by the radicals was determined from the difference in decay rate in a pure Ar plasma and an Ar–NH_3 plasma. If necessary, a minor base line correction was carried out to account for small changes in mirror reflectivity. For the NH_2 measurements an oscillating behavior of the base line signal was observed [which is common for mirrors in the wavelength range around 600 nm (Ref. 34)] that hampered the base line correction procedure and resulted in a slightly lower experimental accuracy compared to the NH measurements.

The NH radical was detected on the (0,0) band of the $A\,^3\Pi \leftarrow X\,^3\Sigma^-$ transition around 340 nm, as shown in Fig. 2(a).[35,36] Apart from transitions of the (0,0) band, this spectrum also shows some hot band transitions of the (1,1) band. The rotational temperature of NH was extracted from the Boltzmann plot shown in Fig. 3(a), in which the statistically weighted integrated absorptions $A_{\mathrm{int}}(K)/(2K+1)$ obtained from the spectrum are plotted as a function of the rotational energy. In this expression, K is the rotational quantum number. This procedure yields a NH rotational temperature of 1920 ± 100 K. For the density measurements, the "isolated" $P_{33}(9)$ absorption line at 339.62 nm (29 444.28 cm^{-1}) was used, as indicated in the spectrum in Fig. 2(a). The density information is determined by scanning the laser over the absorption line and using the integrated absorption cross section, which is calculated from the oscillator strength reported in literature.[36] For the integrated absorption cross section a value of 8.3×10^{-21} $m^2\,cm^{-1}$ was found for the absorption line under investigation (see Appendix A). This method is insensitive to the laser linewidth and the Doppler broadening effect. Doppler broadening was used to determine the kinetic gas temperature of the NH radicals by deconvoluting the experimental absorption lines into a Lorentzian laser linewidth and a Gaussian Doppler contribution. This procedure, carried out on a set of distinct measurements, yielded a laser linewidth of 0.11 ± 0.01 cm^{-1} at a wavelength of 29 444 cm^{-1} and a NH kinetic gas temperature of 1750 ± 90 K with no clear dependence on the NH_3 flow, as can be seen in Fig. 3(b). The laser linewidth is also consistent with the manufacturer's specifications[37] and with earlier data obtained for this laser system.[33] The NH kinetic gas temperature is in fair agreement with the rotational temperature and it reflects the gas temperature in the plasma expansion as thermalization occurs quickly under the conditions used. The gas temperature is also in good agreement with previous measurements in plasmas of different gas mixtures.[33] The NH_2 radical was detected at the (0,9,0)-(0,0,0) band of the $\tilde{A}\,^2A_1 \leftarrow \tilde{X}\,^2B_1$ transition at ~597 nm (Refs. 38 and 39) as shown in Fig. 2(b)

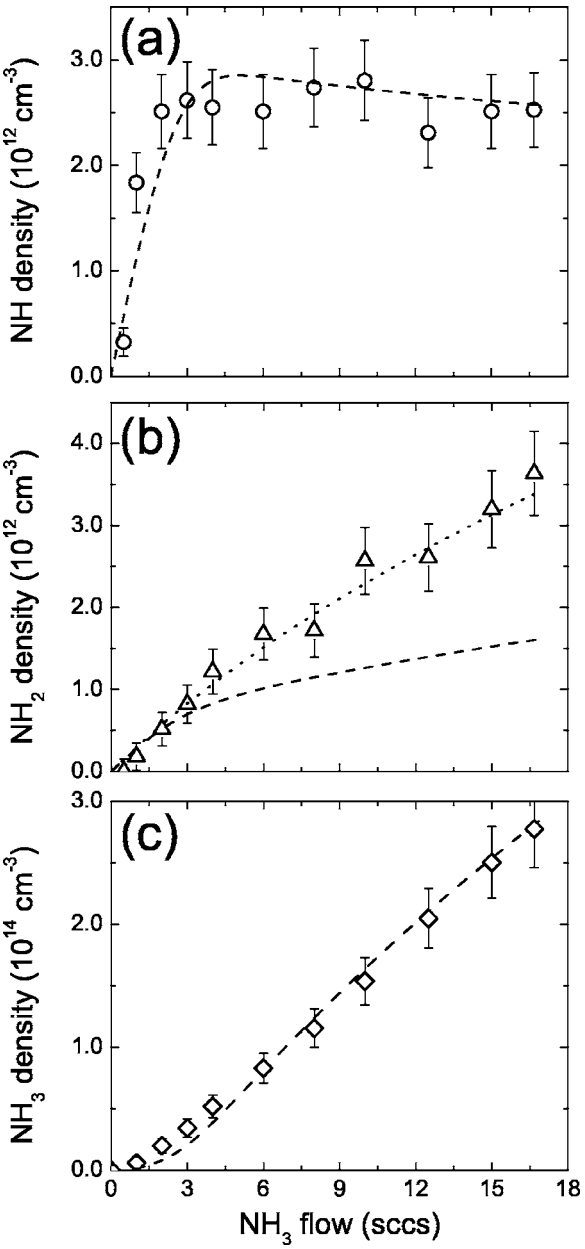

FIG. 4. (a) The NH, (b) NH_2, and (c) NH_3 density as a function of the injected NH_3 flow. The NH and NH_2 density have been measured by cavity ringdown spectroscopy, while the NH_3 density has been calculated from the partial NH_3 density taking into account its consumption as measured by mass spectrometry. The dashed lines are simulation results from a simple one-dimensional plug down model using literature values for the reaction rates. The dotted line shows the modeled NH_2 density when the rate of reaction $R4$ ($NH_3+H \rightarrow NH_2+H_2$) is set to a value that is a factor of 7.5 higher than reported in the literature. For this higher rate, no change in the modeled NH density is observed, while the change in the modeled NH_3 density is negligible.

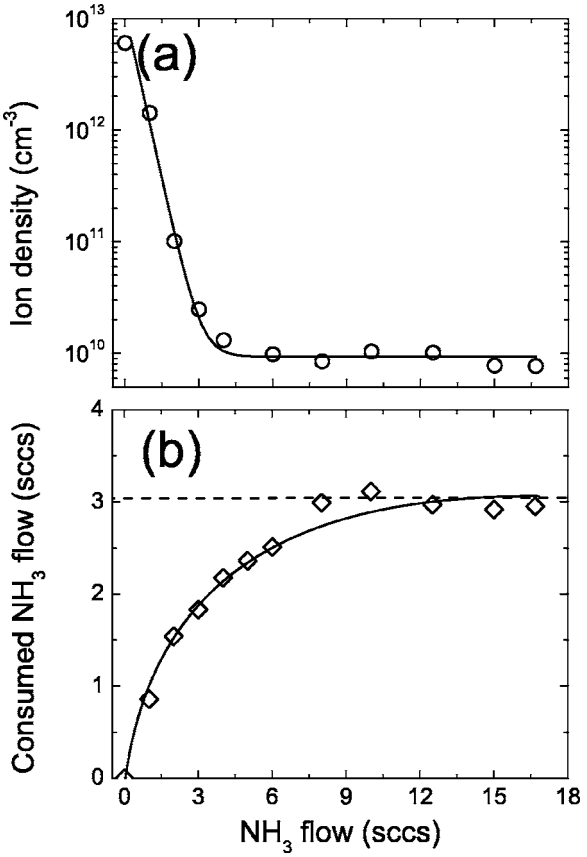

FIG. 5. (a) The ion density and (b) the equivalent flow of consumed NH_3 as a function of the NH_3 flow. The ion density was measured by means of Langmuir probe measurements and the consumed NH_3 flow was determined by means of mass spectrometry experiments. The lines serve as a guide to the eye.

and the isolated $\Sigma^P Q_{1,7}$ absorption line at 597.97 nm (16 739.90 cm^{-1}) (Ref. 40) was used for the density measurements using a procedure similar to the one for NH. From the oscillator strength[39] an integrated absorption cross section of 7.4×10^{-21} m^2 cm^{-1} was deduced for this particular absorption line.

The total NH and NH_2 densities were calculated by taking into account the densities in all possible states assuming a Boltzmann rotational distribution and a rotational temperature of 1750 K. For NH and NH_2, the density in the hot bands was also taken into account by assuming equal temperatures for rotation and vibration and using the vibrational energies reported in the literature.[35,41] The density in the hot bands is approximately 8% of the total density for NH and approximately 39% for NH_2. In Appendixes A and B the derivation of the integrated absorption cross sections and the calculation of the corresponding total densities of NH and NH_2 are given. The largest uncertainty in the absolute values of the densities reported is generated by the assumption about the absorption path length for the radicals in the plasma, which is estimated to be 30 cm.[42] This error can be as large as a factor of 3 for the local absolute densities. Finally, it is important to note that optical saturation can be neglected for both NH and NH_2 as was verified by measuring the absorption line intensities for both radicals as a function of the laser energy coupled into the cavity.

IV. NH AND NH_2 DENSITIES AND PLASMA CHEMISTRY

Figure 4 shows the absolute densities of the NH and NH_2 radicals and the NH_3 molecules in the expanding $Ar-NH_3$ plasma as a function of the NH_3 flow injected through the injection ring. The argon flow used is 55 sccs, the arc current is 45 A, and the downstream pressure is 20 Pa. The radicals were measured at 36 cm from the plasma source whereas the NH_3 density is calculated from the partial

TABLE I. Reactions and rate constants.

	Reaction		Branching	Rate constant ($cm^3\ s^{-1}$)	Reference
*R*1	$Ar^+ + NH_3$	$\rightarrow Ar + NH_3^+$	87%	1.84×10^{-9}	44
		$\rightarrow Ar + NH_2^+ + H$	7%		
		$\rightarrow ArH^+ + NH_2$	6%		
*R*2	$NH_3^+ + e$	$\rightarrow NH_2 + H$	···	1.8×10^{-7}[a]	
		$\rightarrow NH + pH_2 + (2-2p)H$ $(p=0,1)$	···		
		$\rightarrow N + qH_2 + (3-2q)H$ $(q=0,1)$	···		
*R*3	$NH_3^+ + NH_3$	$\rightarrow NH_4^+ + NH_2$		1.7×10^{-9}	50
*R*4	$NH_3 + H$	$\rightarrow NH_2 + H_2$		4×10^{-12} (3×10^{-11}[b])	49
*R*5	$NH_4^+ + e$	$\rightarrow NH_3 + H$	85% (69%)[c]	1.8×10^{-7}[a]	51 and 54
		$\rightarrow NH_2 + H + H$	13% (21%)[c]		
		$\rightarrow NH_2 + H_2$	2% (10%)[c]		
*R*6	$NH_2^+ + e$	$\rightarrow NH + H$	34%	1.8×10^{-7}[a]	54
		$\rightarrow N + H + H$	66%		
		$\rightarrow N + H_2$	0%		
*R*7	$NH^+ + e$	$\rightarrow N + H$		1.8×10^{-7}[a]	
*R*8	$ArH^+ + e$	$\rightarrow Ar + H$		1.8×10^{-7}	55

[a]Estimated rate constant for dissociative recombination reactions.
[b]This value is used in the model calculations shown by the dotted line in Fig. 4(b).
[c]In the model, the branching ratios reported in Ref. 51 were used. These are in fair agreement with earlier results reported in Ref. 54 that are denoted between brackets.

NH_3 density taking into account its consumption as measured by mass spectrometry at 56 cm from the plasma source. The NH density increases rapidly with increasing NH_3 flow and saturates at a level of $\sim2.5\times10^{12}\ cm^{-3}$ for NH_3 flows greater than 3 sccs. Initially, the NH_2 density also increases fast with the NH_3 flow, but for flows higher than 3 sccs the NH_2 density increases more gradually. The NH_2 density shows no saturation and reaches a maximum level of $\sim3.5\times10^{12}\ cm^{-3}$ for the experimental conditions used. The NH_3 density increases almost linearly with the NH_3 flow showing a deviation at low NH_3 flows, where the consumption of NH_3 in the plasma is significant [see Fig. 5(b)]. The maximum NH_3 density is approximately $3\times10^{14}\ cm^{-3}$, which is substantially higher than the NH and NH_2 densities. Within the experimental accuracy, we obtained similar results for both ring injection and nozzle injection of NH_3.

The dissociation of NH_3 is ruled by reactive species emanating from the plasma source, such as Ar^+, metastable argon atoms, Ar^m, and electrons. In the following, we show that argon ions most likely govern the dissociation of NH_3, as is the case in most plasma processes using the ETP source operated on argon. Electron-induced dissociation and ionization of NH_3 are not very important due to the low electron temperatures ($\sim$0.3 eV) in the expanding thermal plasma. Figure 5(a) shows the ion density determined by Langmuir probe measurements for an arc current of 45 A. The ion density (and electron density) in a pure Ar plasma is very high[43] and corresponds to an Ar^+ flow emanating from the source of 2–3 sccs.[29,30] When NH_3 is injected downstream in the plasma, the ion density decreases drastically until it has decreased about three orders of magnitude for NH_3 flows $>$3 sccs. This drastic decrease of the ion density can be attributed mainly to the reaction mechanism, in which Ar^+ ions undergo charge-transfer reactions with NH_3 producing predominantly NH_3^+ (for other branching products see Table I),

$$Ar^+ + NH_3 \rightarrow Ar + NH_3^+, \tag{1}$$

with a reaction rate constant of $1.84\times10^{-9}\ cm^3\ s^{-1}$.[44] Subsequently, the molecular ions produced recombine dissociatively with electrons,

$$\begin{aligned} &\rightarrow NH_2 + H, \\ NH_3^+ + e \rightarrow\ &NH + pH_2 + (2-2p)H \quad (p=0,1), \\ &\rightarrow N + qH_2 + (3-2q)H \quad (q=0,1). \end{aligned} \tag{2}$$

These dissociative recombination reactions typically have a rate constant of $1\times10^{-7}\hat{T}_e^{1/2}\ cm^3\ s^{-1}$,[45] which leads to a rate of $1.8\times10^{-7}\ cm^3\ s^{-1}$ for an electron temperature $\hat{T}_e$ of 0.3 eV. The combination of these two reactions with their high reaction rates explains the very fast decrease in ion density when going from a pure Ar plasma to an Ar–NH_3 plasma. Penning ionization of NH_3 by argon metastables is not important because the Ar^m density in the expanding thermal plasma is typically more than a factor of 10 lower than the density of Ar^+ ions,[31,46] and the reaction rate [$4.2\times10^{-11}\ cm^3\ s^{-1}$ (Ref. 47)] is also considerably smaller than the one of reaction (1).

More evidence for the fact that the argon ions dominate the NH_3 dissociation is obtained by considering the consumed NH_3 flow, which is calculated by multiplying the relative NH_3 consumption with the injected NH_3 flow. Figure 5(b) shows that the consumed NH_3 flow saturates at $\sim$3 sccs, which is, within the experimental accuracy, slightly higher or equivalent to the Ar^+ ion flow emanating from the plasma source (see Sec. II). The NH_3 consumption saturates relatively slow (for an NH_3 flow of $\sim$7 sccs), which might

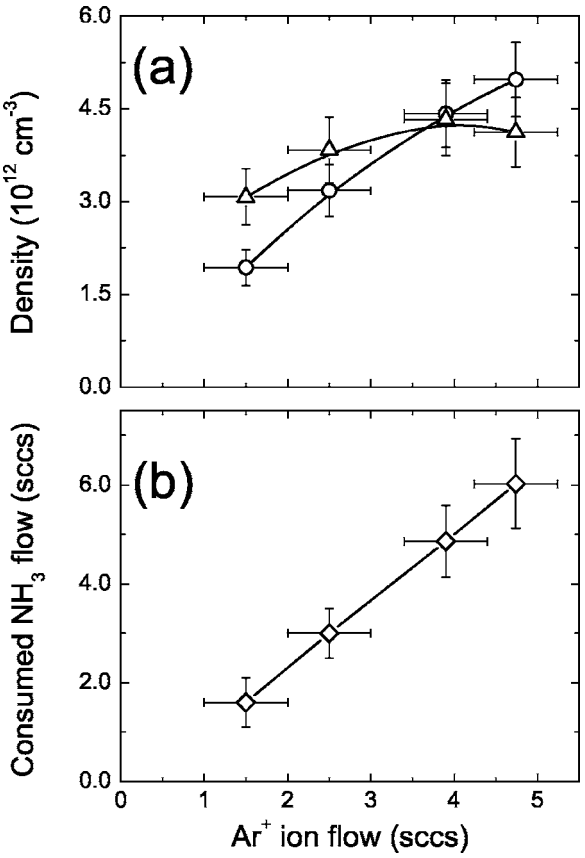

FIG. 6. (a) The NH (circles) and NH_2 (triangles) density and (b) the consumed NH_3 flow as a function of the Ar^+ ion flow emanating from the plasma source. The lines serve as a guide to the eye.

indicate that a small amount of the NH_3 is dissociated by radicals produced by the initial NH_3 dissociation reactions. For completeness, we also mention that pyrolysis of NH_3 molecules due to the relatively high plasma temperatures can be neglected as this reaction has a rate constant below 1×10^{-18} cm^3 s^{-1} for a gas temperature of 1750 K.[48] For this gas temperature, also the dissociation of NH_3 by hydrogen atoms, which are produced by other NH_3 dissociation reactions, does not seem to play a significant role based on its relatively low reaction rate of $\sim 4 \times 10^{-12}$ cm^3 s^{-1},[49] but this reaction will be reconsidered below.

To further test our hypothesis that the NH_3 dissociation is dominated by Ar^+ ions, we measured the NH and NH_2 densities for varying Ar^+ ion flow from the ETP source by changing the plasma current. The argon-ion flow is approximately linear with the plasma current and ranges from $\sim$1.6 sccs at a current of 30 A to $\sim$5 sccs at a current of 70 A. Figure 6(a) shows the NH and NH_2 densities as a function of the plasma current for high NH_3 flows (such that NH_3 is abundantly present and therefore not a limiting factor), and Fig. 6(b) shows the consumed NH_3 flow calculated from mass spectrometry data. Taking into account the experimental uncertainty in the measured Ar^+ flow, both the NH density and the consumed NH_3 flow increase linearly with the Ar^+ flow reaching a density of $\sim 5 \times 10^{12}$ cm^{-3} and a consumed flow of $\sim$6 sccs, respectively. The NH_2 density, however, increases initially and subsequently remains constant at $\sim 4 \times 10^{12}$ cm^{-3}.

The NH density shows a first-order dependence on the Ar^+ flow. This behavior can be explained by NH production via the reaction sequence given by reactions (1) and (2). Furthermore, the NH radicals are not lost in gas phase reactions with NH_3 as can be deduced from the saturation of the NH density as a function of the NH_3 flow in Fig. 4. The density of the NH_2 radical on the other hand shows a less pronounced dependence on the Ar^+ flow. This suggests that the generation of NH_2 radicals is controlled by a different reaction mechanism than the production of NH radicals. A reaction that can play a significant role in the production of NH_2 is the reaction between ammonia ions and molecules,

$$NH_3^+ + NH_3 \rightarrow NH_4^+ + NH_2, \tag{3}$$

which has a reaction rate of 1.7×10^{-9} cm^3 s^{-1}.[50] For high NH_3 flows, when the ion and electron densities are significantly reduced, this reaction becomes competitive with the dissociative recombination reaction of NH_3^+. On the basis of the reaction rates, it can be deduced that this will happen when the ratio of the electron density over the NH_3 density is below $\sim$0.01 (i.e., for an NH_3 flow of $> \sim 3$ sccs). This reaction might therefore explain the gradual increase in the NH_2 density for higher NH_3 flows, which is not observed for the NH density. The NH_4^+ ion formed in this reaction can also recombine dissociatively with electrons, mainly leading to NH_3+H and to a somewhat lesser extent to NH_2 and 2H.[51]

The feasibility of the proposed reaction pathway is investigated by a one-dimensional plug down model. For the type of plasma expansions addressed in this study, such plug down models have been very valuable in gaining insight into the plasma chemistry.[52,53] In the one-dimensional model, the species in the expansion region are produced and consumed by reactions in a forward chemistry as a function of the axial position from the plasma source. The initial conditions are set in terms of the initial ion and NH_3 flows, and it is assumed that the forward velocity and beam diameter are constant. Furthermore, we want to stress that no recirculation of background gas species is included, while also no reactions of species at the reactor walls are explicitly taken into account. Table I shows the reactions that are included in the model with the corresponding reaction rates taken from the literature. For the dissociative recombination reactions, a rate of 1.8×10^{-7} cm^3 s^{-1} has been assumed as discussed earlier. The model results are shown by the dashed lines in Fig. 4 and the trends for NH and NH_3 show a good agreement with the experimental data. For NH_2, however, the model predicts significantly lower NH_2 densities at high NH_3 flows compared to experimental results.

In the model, the branching ratio of the dissociative recombination reaction of NH_3^+ [reaction (2)], which is not known in the literature, was set to 80% NH production and 20% NH_2 production, neglecting the channel resulting in N radicals. This ratio was primarily chosen to reproduce the experimental NH density. Setting the branching ratio to a different value cannot account for the observed NH_2 increase for high NH_3 flows. Also reaction (3) was taken into account in the model, but it cannot fully explain the observed increase of the NH_2 density for high NH_3 flows whereas changes in the rate of this reaction will immediately affect

the modeled NH density. Therefore, another reaction seems to play an important role in the NH_2 production for high NH_3 flows. Although several reactions might contribute to the NH_2 density, we have focused on the reaction of NH_3 with atomic H,

$$NH_3 + H \rightarrow NH_2 + H_2, \tag{4}$$

which has a rather low rate constant of 4.0×10^{-12} cm^3 s^{-1} (Ref. 49) for ground-state reactants. However, this rate, might be substantially higher in the presence of energetic atomic H and rovibrationally excited NH_3^{rv}. In our case, energetic atomic H is primarily produced as a product of the exoergic dissociative recombination reactions in the NH_3 dissociation process, while dissociative recombination of NH_4^+ probably yields NH_3^{rv}.[51] Therefore, reaction (4) is expected to be a good candidate to explain the discrepancy between the modeled and experimental NH_2 densities. When reaction (4) is implemented in the model, good agreement with the experimental data can be achieved for a reaction rate that is a factor of 7.5 higher than the literature value (see Fig. 4). Such an enhancement in reaction rate seems not inconceivable. Reaction (4), as a reaction between NH_3 and atomic H produced from other NH_3 dissociation reactions, might also explain the fact that the consumed NH_3 flow appears to be slightly higher than the Ar^+ ion flow from the plasma source [see Fig. 6(b)] as well as the slow saturation of the consumed NH_3 flow [see Fig. 5(b)].

From the above, it can be concluded that good agreement between the experimental data and the results of a simple plug down model can be obtained by including the reactions in Table I and the corresponding rates reported in the literature. Only to explain the production of NH_2 a higher rate constant for reaction (4) was used. However, we stress that in the model not all possible reactions have been considered. For example, the reactions of NH and NH_2 with NH_3, with themselves, and with other plasma radicals have not been addressed. This seems to be justified on the basis of the reaction rates reported[47] and the (expected) radical densities. Also the surface loss of radicals has not been addressed, as no data are available for the surface reactivity of NH and NH_2 on the stainless-steel reactor walls. However, from the data of Fisher and co-workers[19–21] it seems that the radicals are not very reactive with the surface. Finally, from the radical densities and NH_3 consumption measured, it can be inferred that a significant amount of the consumed NH_3 flow has to be converted into other stable species in the plasma, such as N_2 and H_2 molecules. These and other aspects will be addressed in future studies, while the NH and NH_2 density will also be investigated for the ammonia-silane plasma to address the importance of NH and NH_2 for silicon nitride film growth.

V. CONCLUSIONS

The dissociation of NH_3 in an expanding $Ar-NH_3$ plasma jet created by the ETP technique was investigated with respect to NH and NH_2 radical production. The NH and NH_2 radicals were measured by cavity ringdown spectroscopy for different NH_3 flows and plasma source currents. For NH, densities up to $\sim5\times10^{12}$ cm^{-3} were found when using a high NH_3 flow and plasma source current. The maximum density of NH_2 is $\sim4\times10^{12}$ cm^{-3}. By combining the NH and NH_2 density information with ion density and NH_3 consumption measurements, it was concluded that NH is directly produced through Ar^+ ions from the source in a charge-transfer and dissociative recombination reaction. The situation for NH_2 is more complex and appears to involve ion-molecule reactions between NH_3^+ and NH_3 and possibly H abstraction of NH_3 by atomic H. The results were based on and corroborated by a simple one-dimensional plug down model, which captures the key plasma chemical reactions in terms of NH and NH_2 production in the plasma. Furthermore, from the cavity ringdown measurements a kinetic gas temperature and rotational temperature of 1750 ± 100 and 1920 ± 100 K were found for NH, respectively.

ACKNOWLEDGMENTS

The authors thank M. J. F. van de Sande, J. F. C. Jansen, A. B. M. Hüsken, and H. M. M. de Jong for their skillful technical assistance. This study has been supported by the Netherlands Foundation for Fundamental Research on Matter (FOM) and by the Netherlands Ministry of Economic Affairs, the Ministry of Education, Culture, and Science, and the Ministry of Public Housing, Physical Planning, and Environment (E.E.T.-project "HR-CEL"). The research of one of the authors (W.K.) has been made possible by a fellowship of the Royal Netherlands Academy of Arts and Sciences (KNAW).

APPENDIX A: CROSS SECTION OF THE $A\,^3\Pi(\nu'=0)\leftarrow X\,^3\Sigma^-(\nu''=0)P_{33}(9)$ TRANSITION OF NH AT 29 444.277 CM^{-1}

For NH the integrated cross section can be calculated from the Einstein coefficient for spontaneous emission on the basis of the information reported by Lents[36] and Schadee.[56] The integrated absorption cross section of a molecule σ_{int} can be directly related to the Einstein coefficient for spontaneous emission A_{ki} (Ref. 57),

$$\sigma_{int} = \int \sigma_{ik}(\nu)\mathrm{d}\nu = \frac{g_k}{g_i}\frac{c^2}{8\pi\nu^2}A_{ki}, \tag{A1}$$

where c is the speed of light, g_i and g_k are the degeneracies of the lower i and upper level k, and ν is the transition frequency. Subsequently, the Einstein coefficient for emission A_{ki} can be related to the electronic-vibrational transition probability A_{00} by the following expression (Ref. 36):

$$A_{ki} = A_{00}\frac{P_{33}(J)}{g_e'[2(J-1)+1](2S'+1)}, \tag{A2}$$

where $P_{33}(J)$ is the Hönl-London factor for lines in the P_{33} branch of the $A\,^3\Pi$-$X\,^3\Sigma^-$ transition, g_e' is the electron degeneracy of the upper level, S' is the total spin of the upper state, and J is the quantum number of the total angular momentum of the lower level. In the subsequent derivation, singly primed coefficients pertain to the upper Π state and doubly primed quantities to the lower Σ state. The Hönl-London factor $P_{33}(J)$ is given by Schadee,[56]

$$P_{33}(J) = \frac{(J-1)(J+1)[(J-2)u'_{3+}(J-1)g''(J) + 4(J-1)\sqrt{J(J+1)}s''(J) + Ju'_{3-}(J-1)g''(J)]^2}{8JC'_3(J-1)}, \tag{A3}$$

with the following coefficients:

$$g(J) = \left[\frac{F_2(J) - F_1(J)}{F_3(J) - F_1(J)}\right]^{1/2}, \tag{A4}$$

$$s(J) = \left[\frac{F_3(J) - F_2(J)}{F_3(J) - F_1(J)}\right]^{1/2}, \tag{A5}$$

$$u_{3+}(J) = [(Y-2)^2 + 4J(J+2)]^{1/2} + (Y-2), \tag{A6}$$

$$u_{3-}(J) = [(Y-2)^2 + 4J(J+2)]^{1/2} - (Y-2), \tag{A7}$$

$$C_3(J) = Y(Y-4)(J-1)(J+2) + 2(2J+1)J(J+1)(J+2) - (Y-2)[(Y-2)^2 + 4J(J+2)]^{1/2} + Y(Y-4) - 4(J+1), \tag{A8}$$

$$F_2(J) - F_1(J) = \{[B_\nu - (1/2)\gamma - \lambda]^2 + 4J(J+1) \times [B_\nu - (1/2)\gamma]^2\}^{1/2} - [B_\nu - (1/2)\gamma - \lambda], \tag{A9}$$

$$F_3(J) - F_2(J) = \{[B_\nu - (1/2)\gamma - \lambda]^2 + 4J(J+1) \times [B_\nu - (1/2)\gamma]^2\}^{1/2} + [B_\nu - (1/2)\gamma - \lambda], \tag{A10}$$

$$F_3(J) - F_1(J) = 2\{[B_\nu - (1/2)\gamma - \lambda]^2 + 4J(J+1) \times [B_\nu - (1/2)\gamma]^2\}^{1/2}. \tag{A11}$$

The molecular constants γ represents the spin-rotation interaction, λ is the splitting constant, B_v the rotational constant, and Y represents the coupling between the nuclear spin S and the orbital angular momentum Λ. The electron degeneracies of the Σ and Π states are $(2S+1)$ and $2(2S+1)$, respectively.[58] Using the molecular constants of the electronic states ($A\ ^3\Pi$ and $X\ ^3\Sigma^-$) of the NH radical reported by Brazier *et al.*[35] and the electronic-vibrational transition probability A_{00} reported by Lents,[36] we can calculate the Einstein coefficient for emission of the $P_{33}(J=9)$ line,

$$A_{ki} = 6.07 \times 10^4\ \mathrm{s}^{-1}. \tag{A12}$$

Using Eq. (A1) and $g_k = 2(J-1)+1$ and $g_i = 2J+1$ with $J=9$ we find for the integrated absorption cross section,

$$\sigma_{\mathrm{int}} = 2.49 \times 10^{-10}\ \mathrm{m}^2\ \mathrm{Hz}. \tag{A13}$$

The peak absorption cross section for a gas temperature T can now be calculated by incorporating the Gaussian lineshape function $\Phi(0,a)$ that depends on the pressure-broadening parameter a,[39,48]

$$\sigma_{\mathrm{peak}} = \sigma_{\mathrm{int}}\Phi(0,a). \tag{A14}$$

For the low working pressures in our experimental conditions, pressure broadening is negligible[59] and $\Phi(0,a)$ can be written as a function of the Doppler width $\Delta\nu_D$,

$$\Phi(0,a) = \sqrt{\frac{4\ln 2}{\pi}}\frac{1}{\Delta\nu_D}. \tag{A15}$$

$\Delta\nu_D$ is the full width at half maximum of the Doppler-broadened line profile and can be written as

$$\Delta\nu_D = \frac{\nu}{c}\sqrt{\frac{8kT\ln 2}{m}} = 7.16 \times 10^{-7}\nu\sqrt{\frac{T}{M}}, \tag{A16}$$

with k as Boltzmann's constant, m the mass of the NH molecule, T the gas temperature (in Kelvin), and M the molar mass of NH. This formula results in a peak absorption cross section of the $A\ ^3\Pi(\nu'=0) \leftarrow X\ ^3\Sigma^-(\nu''=0)P_{33}(9)$ line at $T = 1750$ K of

$$\sigma_{\mathrm{peak}} = 3.43 \times 10^{-20}\ \mathrm{m}^2. \tag{A17}$$

The density of NH in the $A\ ^3\Pi(\nu'=0) \leftarrow X\ ^3\Sigma^-(\nu''=0)P_{33}(9)$ transition can be calculated from measured integrated absorption A_{int},

$$n_{\mathrm{NH},J=9} = \frac{A_{\mathrm{int}}}{\sigma_{\mathrm{int}}l}, \tag{A18}$$

where l is the length of the absorption path in the cavity (30 cm). Assuming a Maxwell-Boltzmann distribution for densities in the rotational and vibrational states, we can calculate the total NH density,

$$n_{\mathrm{NH}} = \frac{n_{\mathrm{NH},J=9}}{f_b}, \tag{A19}$$

where the f_b is the Boltzmann fraction which is taken from Herzberg,[60]

$$f_b = \frac{2J+1}{Q_rQ_v}\exp\left[-\frac{E_{\mathrm{rot}}(K)}{kT_{\mathrm{rot}}}\right]\exp\left[-\frac{E_{\mathrm{vib}}(n)}{kT_{\mathrm{vib}}}\right]. \tag{A20}$$

Q_r and Q_v are the rotational and vibrational partition functions, respectively, and $E_{\mathrm{vib}}(n)$ and $E_{\mathrm{rot}}(K)$ the vibrational energy and the rotational energy,

$$E_{\mathrm{vib}}(n) = hc\omega_1(n+1/2), \tag{A21}$$

$$E_{\mathrm{rot}}(K) = hcB_\nu K(K+1). \tag{A22}$$

h is Planck's constant, ω_1 the vibrational constant, n is the vibrational quantum number, and K is the rotational quantum number of the lower level apart from spin. The vibrational partition function including the zero-point energy is given by Herzberg,[60]

$$Q_v = \frac{\exp\left[-\frac{hc\omega_1}{2kT_{\text{vib}}}\right]}{1-\exp\left[-\frac{hc\omega_1}{kT_{\text{vib}}}\right]}. \tag{A23}$$

For the diatomic NH, the rotational partition function can be approximated by the classical expression,[60]

$$Q_r = \frac{kT}{hcB_v}. \tag{A24}$$

Using molecular constants reported by Brazier *et al.*[35] and assuming the rotational and vibrational temperatures to be equal to the gas temperature ($T=1750$ K in the present work), the total NH density (m^{-3}) can be calculated as a function of the measured integrated absorption $A_{\text{int}}(cm^{-1})$,

$$n_{\text{NH}} = \frac{n_{\text{NH},J=9}}{f_b} = 7.39\times10^{21}A_{\text{int}}. \tag{A25}$$

APPENDIX B: CROSS SECTION OF THE $\tilde{A}\,^2A_1(0,9,0)\leftarrow\tilde{X}\,^2B_1(0,0,0)\Sigma^P\,Q_{1,7}$ TRANSITION OF NH_2 AT 16 739.90 CM^{-1}

For NH_2, the integrated cross section can be calculated from information on the oscillator strength reported by Votsmeier *et al.*[39] and the molecular constants reported by Green and Miller.[41] The relation between the integrated absorption cross section of a molecule σ_{int} and the oscillator strength f_{ik} of the transition is given by[57]

$$\sigma_{\text{int}} = \frac{e^2}{4\varepsilon_0 m_e c} f_{ik}. \tag{B1}$$

Using the fundamental physical constants for the electron mass m_e elementary charge e, the dielectric constant ε_0, the speed of light c, and the oscillator strength $f_{ik}=8.36\times10^{-5}$ reported by Votsmeier *et al.*,[39] we find the following value for the integrated absorption cross section:

$$\sigma_{\text{int}} = 2.21\times10^{-10}\ \text{m}^2\ \text{Hz}. \tag{B2}$$

Using a similar procedure as for the NH radical in the previous section [Eqs. (A14)–(A16)], one can calculate the peak absorption cross section σ_{peak} for the $\tilde{A}\,^2A_1(0,9,0)\leftarrow\tilde{X}\,^2B_1(0,0,0)\Sigma^P\,Q_{1,7}$ transition of NH_2 by incorporating the line-shape function $\Phi(0,a)$ for a gas temperature of 1750 K [Eq. (A15)],

$$\sigma_{\text{peak}} = 5.53\times10^{-20}\ \text{m}^2. \tag{B3}$$

To obtain the total density of NH_2, we adapt a similar procedure as for the NH radical [Eqs. (A18) and (A19)]. The Boltzmann fraction f_b for NH_2 is given by Green and Miller[41] and Kohse-Höinghaus *et al.*,[61]

$$f_b = \frac{3}{4}\frac{(2J''+1)}{g''Q_rQ_v}\exp\left[-\frac{E_{\text{rot}}}{kT_{\text{rot}}}\right]\exp\left[-\frac{E_{\text{vib}}}{kT_{\text{vib}}}\right]. \tag{B4}$$

Q_r and Q_v are the rotational and vibrational partition functions and J'' and g'' are the total rotational quantum numbers including spin and the electron-spin degeneracy of the lower state. The factor 3/4 occurs due to the nuclear spin of the H atoms. The vibrational energy E_{vib} for the NH_2 molecule is given by[60]

$$E_{\text{vib}} = hc\omega_1(n_1+1/2)+hc\omega_2(n_2+1/2)+hc\omega_3(n_3+1/2), \tag{B5}$$

with ω_1, ω_2, and ω_3 the vibrational constants and n_1, n_2, and n_3 the vibrational quantum numbers of the lower state. The rotational energy is given by the following formula:

$$E_{\text{rot}} = hcF(J), \tag{B6}$$

where $F(J)$ is the experimentally determined rotational term value reported by Ross *et al.*.[38] The vibrational partition function including the zero-point energy of the vibration is given by Green and Miller,[41]

$$Q_v = \frac{\exp\left[-\frac{hc\omega_1}{2kT}\right]}{1-\exp\left[-\frac{hc\omega_1}{kT}\right]}\frac{\exp\left[-\frac{hc\omega_2}{2kT}\right]}{1-\exp\left[-\frac{hc\omega_2}{kT}\right]}\frac{\exp\left[-\frac{hc\omega_3}{2kT}\right]}{1-\exp\left[-\frac{hc\omega_3}{kT}\right]}. \tag{B7}$$

For NH_2, which is an asymmetric top molecule, the rotational partition function Q_r can be estimated by[41,60]

$$Q_r = \frac{\sqrt{\pi}}{\sigma}\sqrt{\frac{8\pi^2I_AkT}{h^2}}\sqrt{\frac{8\pi^2I_BkT}{h^2}}\sqrt{\frac{8\pi^2I_CkT}{h^2}}. \tag{B8}$$

In this equation, σ is the symmetry number and I_A, I_B, and I_C are the moments of inertia of the NH_2 molecule. The symmetry number σ is equal to 2 and the electron spin degeneracy g'' is equal to 1, because the measured line is in fact a spin-split doublet, which is not resolved by the measurement. Using the moments of inertia and the vibrational frequencies reported by Green and Miller[41] and assuming equal temperatures for rotation and vibration (1750 K), we can calculate the total NH_2 density (m^{-3}) as a function of the measured integrated absorption $A_{\text{int}}(cm^{-1})$,

$$n_{\text{NH}_2} = \frac{A_{\text{int}}}{\sigma_{\text{int}}l}\frac{1}{f_b} = 4.95\times10^{22}A_{\text{int}}. \tag{B9}$$

[1] J. E. Klemberg-Sapieha, O. M. Küttel, L. Martinu, and M. R. Wertheimer, J. Vac. Sci. Technol. A **9**, 2975 (1991).
[2] J. Kurdi, H. Ardelean, P. Marcus, P. Jonnard, and F. Arefi-Khonsari, Appl. Surf. Sci. **189**, 119 (2002).
[3] A. Lu and R. Sipehia, Biomaterials **22**, 1439 (2001).
[4] E. F. Castro Vidaurre, C. A. Achete, R. A. Simão, and A. C. Habert, Nucl. Instrum. Methods Phys. Res. B **175–177**, 732 (2001).
[5] E. S. Aydil, K. P. Giapis, R. A. Gottscho, V. M. Donnelly, and E. Yoon, J. Vac. Sci. Technol. B **11**, 195 (1993).
[6] C.-M. Yu, H.-C. Lin, T.-Y. Huang, and T.-F. Lei, J. Electrochem. Soc. **150**, G843 (2003).
[7] Y.-S. Lai, K.-J. Chen, and J. S. Chen, J. Appl. Phys. **91**, 6428 (2002).
[8] J. C. Wang, D. C. Shie, T. F. Lei, and C. L. Lee, Electrochem. Solid-State Lett. **6**, F34 (2003).
[9] M. Chhowalla *et al.*, J. Appl. Phys. **90**, 5308 (2001).
[10] Z. P. Huang, J. W. Xu, Z. F. Ren, J. H. Wang, M. P. Siegal, and P. N. Provencio, Appl. Phys. Lett. **73**, 3845 (1998).
[11] Y. J. Lee and S.-W. Kang, Thin Solid Films **446**, 227 (2004).
[12] H. S. Sim, J. H. Park, and Y. T. Kim, Phys. Status Solidi A **201**, R92 (2004).
[13] O.-K. Kwon, S.-H. Kwon, H.-S. Park, and S.-W. Kang, Electrochem. Solid-State Lett. **7**, C46 (2004).
[14] A. G. Aberle, Sol. Energy Mater. Sol. Cells **65**, 239 (2001).

[15]J. Hong, W. M. M. Kessels, W. J. Soppe, A. W. Weeber, W. M. Arnoldbik, and M. C. M. van de Sanden, J. Vac. Sci. Technol. B **21**, 2123 (2003).
[16]D. Stryahilev, A. Sazonov, and A. Nathan, J. Vac. Sci. Technol. A **20**, 1087 (2002).
[17]G. P. Miller and J. K. Baird, J. Phys. Chem. **97**, 10984 (1993).
[18]S. D. Pringle, V. S. Joss, and C. Jones, Surf. Interface Anal. **24**, 821 (1996).
[19]E. R. Fisher, P. Ho, W. G. Breiland, and R. J. Buss, J. Phys. Chem. **96**, 9855 (1992).
[20]P. R. McCurdy, C. I. Butoi, K. L. Williams, and E. R. Fisher, J. Phys. Chem. B **103**, 6919 (1999).
[21]M. L. Steen, K. R. Kull, and E. R. Fisher, J. Appl. Phys. **92**, 55 (2002).
[22]H. Unemoto, K. Ohara, D. Morita, T. Morimoto, M. Yamawaki, A. Masuda, and H. Matsumura, Jpn. J. Appl. Phys., Part 1 **42**, 5315 (2003).
[23]D. L. Smith, A. S. Alimonda, C.-C. Chen, S. E. Ready, and B. Wacker, J. Electrochem. Soc. **137**, 614 (1990).
[24]D. L. Smith, J. Vac. Sci. Technol. A **11**, 1843 (1993).
[25]M. S. Bell, R. G. Lacerda, K. B. K. Teo, N. L. Rupesinghe, G. A. J. Amaratunga, and W. I. Milne, Appl. Phys. Lett. **85**, 1137 (2004).
[26]S. D. Rodgers and S. B. Charnley, Astrophys. J. **546**, 324 (2001).
[27]H. Kawakita *et al.*, Science **294**, 1089 (2001).
[28]J. Hong, W. M. M. Kessels, F. J. H. van Assche, H. C. Rieffe, W. J. Soppe, A. W. Weeber, and M. C. M. van de Sanden, Prog. Photovoltaics **11**, 125 (2003).
[29]W. M. M. Kessels, C. M. Leewis, M. C. M. van de Sanden, and D. C. Schram, J. Appl. Phys. **86**, 4029 (1999).
[30]M. C. M. van de Sanden, R. J. Severens, W. M. M. Kessels, R. F. G. Meulenbroeks, and D. C. Schram, J. Appl. Phys. **84**, 2426 (1998); **85**, 1243 (1999).
[31]A. J. M. Buuron, D. K. Otorbaev, M. C. M. van de Sanden, and D. C. Schram, Phys. Rev. E **50**, 1383 (1994).
[32]K. W. Busch and M. A. Busch, *Cavity-Ringdown Spectroscopy—An Ultratrace-Absorption Measurement Technique* (American Chemical Society, Washington, 1998).
[33]J. P. M. Hoefnagels, Y. Barrell, W. M. M. Kessels, and M. C. M. van de Sanden, J. Appl. Phys. **96**, 4094 (2004).
[34]D. Romanini and K. K. Lehmann, J. Chem. Phys. **99**, 6287 (1993).
[35]C. R. Brazier, R. S. Ram, and P. F. Bernath, J. Mol. Spectrosc. **120**, 381 (1986).
[36]J. M. Lents, J. Quant. Spectrosc. Radiat. Transf. **13**, 297 (1973).
[37]Manual PrecisionScan-D dye laser. Sirah Laser-und Plasmatechnik GmbH, Darmstadt, Germany (1999).
[38]S. C. Ross, F. W. Birss, M. Vervloet, and D. A. Ramsay, J. Mol. Spectrosc. **129**, 436 (1988).
[39]M. Votsmeier, S. Song, D. F. Davidson, and R. K. Hanson, Int. J. Chem. Kinet. **31**, 323 (1999).
[40]This absorption line is in fact a spin doublet that is not resolved by the measurements.
[41]R. M. Green and J. A. Miller, J. Quant. Spectrosc. Radiat. Transf. **26**, 313 (1981).
[42]W. M. M. Kessels, A. Leroux, M. G. H. Boogaarts, J. P. M. Hoefnagels, M. C. M. van de Sanden, and D. C. Schram, J. Vac. Sci. Technol. A **19**, 467 (2001).
[43]The ion density decreases exponentially downstream due to the very effective charge-transfer reactions of the ion with the injected NH_3 molecules, followed by very fast dissociative recombination of the resulting molecular ion.
[44]R. Derai, G. Mauclaire, and R. Marx, Chem. Phys. Lett. **86**, 275 (1982).
[45]J. Perrin, O. Leroy, and M. C. Bordage, Contrib. Plasma Phys. **36**, 3 (1996).
[46]Argon metastables, Ar^m, in a pure Ar plasma are produced downstream by three-particle recombination of Ar^+ with electrons. When molecular gases are admixed, this reaction channel for Ar^+ loss is highly unlikely and therefore the Ar^m density is lower than the Ar^+ density by more than a factor 10.
[47]M. J. Kushner, J. Appl. Phys. **71**, 4173 (1992).
[48]I. Rahinov, N. Ditzian, A. Goldman, and S. Cheskis, Appl. Phys. B: Lasers Opt. **77**, 541 (2003).
[49]T. Ko, P. Marshall, and A. Fontijn, J. Phys. Chem. **94**, 1401 (1990).
[50]M. P. Skrzypkowski and R. Johnsen, Chem. Phys. Lett. **274**, 473 (1997).
[51]J. Öjekull *et al.*, J. Chem. Phys. **120**, 7391 (2004).
[52]W. M. M. Kessels, J. P. M. Hoefnagels, M. G. H. Boogaarts, D. C. Schram, and M. C. M. van de Sanden, J. Appl. Phys. **89**, 2065 (2001).
[53]J. Benedikt, D. C. Schram, and M. C. M. van de Sanden, J. Phys. Chem. A (in press).
[54]L. Vikor *et al.*, Astron. Astrophys. **344**, 1027 (1999).
[55]R. F. G. Meulenbroeks, A. J. van Beek, A. J. G. van Helvoort, M. C. M. van de Sanden, and D. C. Schram, Phys. Rev. E **49**, 4397 (1994).
[56]A. Schadee, Astron. Astrophys. **41**, 213 (1975).
[57]A. P. Thorne, *Spectrophysics* (Chapman and Hall, London, 1974).
[58]G. Herzberg, *Spectra of Diatomic Molecules* (Van Nostrand, Princeton, 1965).
[59]G. Friedrichs, M. Colberg, M. Fikri, Z. Huang, J. Neumann, and F. Temps, J. Phys. Chem. A **109**, 4785 (2005).
[60]G. Herzberg, in *Molecular Spectra and Molecular Structure*, Infrared and Raman Spectra of Polyatomic Molecules Vol. II (Van Nostrand, Princeton, 1966).
[61]K. Kohse-Höinghaus, D. F. Davidson, A. Y. Chang, and R. K. Hanson, J. Quant. Spectrosc. Radiat. Transf. **42**, 1 (1989).